

High-gravity intensified iron-carbon micro-electrolysis for degradation of dinitrotoluene

Jiaxin Jing, Weizhou Jiao (✉), Zhixing Li, Kechang Gao, Jingwen Zhang, Gaomiao Ren, Youzhi Liu

Shanxi Province Key Laboratory of Hige-Oriented Chemical Engineering, North University of China, Taiyuan 030051, China

© Higher Education Press 2022

Abstract The application of iron-carbon (Fe-C) micro-electrolysis to wastewater treatment is limited by the passivation potential of the Fe-C packing. In order to address this problem, high-gravity intensified Fe-C micro-electrolysis was proposed in this study for degradation of dinitrotoluene wastewater in a rotating packed bed (RPB) using commercial Fe-C particles as the packing. The effects of reaction time, high-gravity factor, liquid flow rate and initial solution pH were investigated. The degradation intermediates were determined by gas chromatography-mass spectrometry, and the possible degradation pathways of nitro compounds by Fe-C micro-electrolysis in RPB were also proposed. It is found that under optimal conditions, the removal rate of nitro compounds reaches 68.4% at 100 min. The removal rate is maintained at approximately 68% after 4 cycles in RPB, but it is decreased substantially from 57.9% to 36.8% in a stirred tank reactor. This is because RPB can increase the specific surface area and the renewal of the liquid-solid interface, and as a result the degradation efficiency of Fe-C micro-electrolysis is improved and the active sites on the Fe-C surface can be regenerated for continuous use. In conclusion, high-gravity intensified Fe-C micro-electrolysis can weaken the passivation of Fe-C particles and extend their service life.

Keywords high-gravity technology, rotating packed bed, Fe-C micro-electrolysis, dinitrotoluene wastewater, active sites

1 Introduction

Dinitrotoluene is a chemically important intermediate in the production of 2,4,6-trinitrotoluene, drugs, dyes and polymers [1,2]. Dinitrotoluene wastewater is discharged

in large quantities from the refining and washing processes of dinitrotoluene, and approximately 1.2 million tons of soil have been contaminated with explosives in America alone [3]. Thus, many methods have been proposed for degradation of nitroaromatic compounds in the wastewater, mainly including physical methods such as extraction [4,5] and activated carbon adsorption [6], advanced oxidation process such as Fenton oxidation and ozonation [7–10], and microbiological degradation [11,12]. Each method has distinct advantages and disadvantages that make it suitable only for specific applications. For instance, physical methods are applicable to the treatment of high-concentration nitroaromatic compounds that can be recycled for future use. Parham [13] used micron-sized anthracite particles to adsorb nitrobenzene and found that anthracite had strong adsorption capacity, short adsorption time, high efficiency, and strong reusability. Arowo et al. [14] investigated the effectiveness of simultaneous use of ozone and hydrogen peroxide to degrade *o*-phenylenediamine in a simulated wastewater by a rotating packed bed (RPB). The results showed that the degradation efficiency of *o*-phenylenediamine (η), overall gas-phase volumetric mass transfer coefficient ($k_G a$) and chemical oxygen demand reduction (r_{COD}) of ozone and hydrogen peroxide increased by 24.4%, 31.6% and 25.2% compared with O_3 process, indicating that H_2O_2 significantly improved the ozonation capacity of *o*-phenylenediamine. Microbiological degradation is applicable to wastewater treatment where the BOD:COD (biochemical oxygen demand: chemical oxygen demand) ratio is higher than 0.3. Nitroaromatic compounds are stable as the strong electron withdrawing effect of nitro groups can significantly reduce the electron cloud density of the benzene ring. Common oxidation methods such as Fenton oxidation and ozonation may have the problems of low degradation efficiency and high cost [15–17]. Thus, there is a pressing need to find a low-cost and high-efficient method for the treatment of dinitrotoluene wastewater.

Fe–C micro-electrolysis is capable of reducing the $-\text{NO}_2$ on the benzene ring into electron-donating $-\text{NH}_2$, which makes it easier to activate and degrade the benzene ring [18]. A large number of Fe–C galvanic cells are formed and the substituent groups of organic pollutants can be reduced or converted because of the electrochemical corrosion of iron. Thus, Fe–C micro-electrolysis can improve the biodegradability of organic pollutants without requiring additional power supplies and reagents, and it is also known for its high efficiency, wide application, low cost and simple operation. However, many problems remain unresolved for repeated use of Fe–C particles. Yang et al. [19] used Fe–C micro-electrolysis for degradation of amino silicone polymers in a water emulsion, and found that the removal efficiency of chemical oxygen demand was reduced from 60% to 20% after three runs due to deactivation of Fe–C particles. Lai et al. [20] found that the Fe content was decreased but the O content was increased on the surface of reacted Fe–C, and an oxide film composed mainly of Fe_2O_3 and Fe_3O_4 was formed to inhibit the micro-electrolysis. Zhao et al. [21] showed that the charge transfer resistance in micro-electrolysis was reduced in a magnetic field, which could enhance the corrosion of iron and consequently the efficiency of Fe–C micro-electrolysis. However, it remains challenging to regenerate Fe–C particles. Ultrasonic treatment can improve the efficiency of Fe–C micro-electrolysis for degradation of organic wastewater [22,23], as it can remove the metal oxides or deposits on the Fe–C surface [24], resulting in regeneration of reactive sites; and the ultrasonic cavitation effect can cause flow turbulence and high mass transfer, resulting in an increase in the reaction rate of Fe–C micro-electrolysis. However, the high energy consumption and low treatment capacity and efficiency make it less suitable for industrial uses.

In order to improve the passivation and regeneration of Fe–C materials in Fe–C micro-electrolysis, the high-gravity technique [25] is used in this study to intensify Fe–C micro-electrolysis for degradation of dinitrotoluene. In this novel process intensification technique, a high-gravity field is created by the high-speed rotating packing and the liquid flowing in the porous media or pores can be sheared into ultra-thin films or small droplets by the large shear force [26,27]. As a result, the specific surface area is greatly increased and the liquid–solid interface is renewed rapidly [28–30], which can increase the contact of wastewater with Fe–C packing in unit time and ensure a high concentration of organic pollutants on the filler surface for mass transfer. As the rotor filled with Fe–C particles rotates at a high speed, the resulting scouring effect can accelerate the renewal of the interface, prevent the passivation of Fe–C packing and promote the regeneration of reactive sites. The liquid will appear and then disappear instantaneously in an alternative manner on the packing surface under high centrifugal force,

which can prevent the deposition of iron oxides on the surface and thus the passivation of Fe–C packing. In this study, commercial Fe–C materials are used for the treatment of dinitrotoluene wastewater in a high-gravity environment. The effects of various operation parameters, such as initial solution pH, reaction time, high-gravity factor and liquid flow rate, on the removal efficiency of dinitrotoluene are investigated, and the formation mechanism of Fe ions is discussed. This study may contribute to better understanding the passivation of Fe–C materials in Fe–C micro-electrolysis and provide a pretreatment method for deep oxidation of wastewater.

2 Experimental

2.1 Reagents and experimental setup

Dinitrotoluene wastewater was collected from a chemical plant, where $\text{pH} = 1.1$, $\text{COD} = 1630 \text{ mg}\cdot\text{L}^{-1}$, the concentration of nitroaromatic compounds was $200 \text{ mg}\cdot\text{L}^{-1}$, and the main component was dinitrotoluene. Fe–C particles (Fe = 72%, C = 15%, other elements = 13%) were purchased from Environmental Protection Technology Co., Ltd. (Weifang, China). NaOH (AR) was purchased from Tianjin Guangfu Reagent Co., Ltd. (Tianjin, China). H_2SO_4 (AR) was purchased from Xilong Chemical Co., Ltd. (Shantou, China). pH was measured using a pH meter (FE28; Mettler Toledo, Switzerland). RPB was self-made in our laboratory (Taiyuan, China).

2.2 Experimental procedure

The high-gravity intensified Fe–C micro-electrolysis is schematically shown in Fig. 1, and the characteristic parameters of RPB are shown in Table 1.

Two liters of dinitrotoluene wastewater was pumped from the storage tank into RPB through a flow meter at a

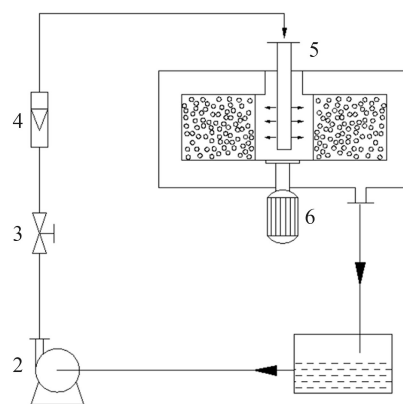


Fig. 1 Schematic view of high-gravity intensified Fe–C micro-electrolysis: 1) reservoir; 2) centrifugal pump; 3) valve; 4) flow meter; 5) RPB; 6) frequency conversion motor.

Table 1 Characteristic parameters of RPB

Characteristic parameter	Value
Rotor inner radius/mm	60
Rotor outer radius/mm	180
Rotor height/mm	30
Packing type	Fe–C particles
Packing porosity/(m ³ ·m ⁻³)	0.49

given speed by using a centrifugal pump, and then uniformly sprayed on the inner edge of the rotor through a liquid distributor. The rotor was filled with Fe–C particles and rotated at a high speed. The liquid was sheared into micro-elements and came into contact with Fe–C particles as it flowed radially from the inner edge to the outer edge of packing. After that, the liquid was thrown to the outer wall and discharged through the outlet for circulation. Samples were taken at given time intervals for measurement of remaining nitro compounds and dissolved iron elements (Fe²⁺ and Fe³⁺) in the wastewater. The removal rate of nitro compounds and the total iron concentration in the solution were used to indicate the removal efficiency of high-gravity intensified Fe–C micro-electrolysis. The experimental parameters, such as reaction time, pH, high-gravity factor and liquid flow rate, were varied to determine the optimal operating conditions. For comparison purposes, 2 L of dinitrotoluene wastewater was placed in a traditional stirred tank reactor (STR) with the same volume of Fe–C particles under stirring conditions for 100 min.

2.3 Analytical methods

The degradation efficiency of high-gravity intensified Fe–C micro-electrolysis was indicated by the removal rate of nitro compounds. The concentration of nitro compounds was measured by reduction-azo spectrophotometry [31], where the relative deviation was 3.5%. The removal rate of nitro compounds was calculated using Eq. (1):

$$\eta(\%) = \frac{c_0 - c_t}{c_0} \times 100, \quad (1)$$

where η (%) is the removal efficiency of nitro compounds, and c_0 and c_t are the concentrations of nitro compounds in the wastewater at the initial time and time t , respectively, mg·L⁻¹.

The electrolysis efficiency of high-gravity intensified Fe–C micro-electrolysis was indicated by the total iron concentration in the supernatant, which was determined by *o*-phenanthroline spectrophotometric method [32].

3 Results and discussion

3.1 Effects of operation parameters

In this study, the effects of reaction time, high-gravity factor (β), liquid flow rate and initial solution pH on the degradation of dinitrotoluene by Fe–C micro-electrolysis in RPB were investigated. The higher the removal rate of nitro compounds and the total iron concentration in the wastewater are, the higher the degradation performance of Fe–C micro-electrolysis will be.

3.1.1 Variations of pH, removal rate of nitro compounds and total iron concentration in the wastewater

Figure 2 shows that the pH of the wastewater and the removal rate of nitro compounds increase continuously, while the total iron concentration first increases and then decreases as the reaction proceeds. Note that the increasing rate of pH is low and thus the pH is still lower than 2 at 70 min, which ensures a high H⁺ concentration in the solution and prevents the formation of an oxide film on the packing surface. Fe can react with H⁺ to form active groups such as Fe²⁺ and nascent [H], which in turn undergo reduction reactions with organic pollutants in the wastewater [33]. As a result, the H⁺ concentration would decrease as the reaction proceeds, and at pH > 3, Fe³⁺ can

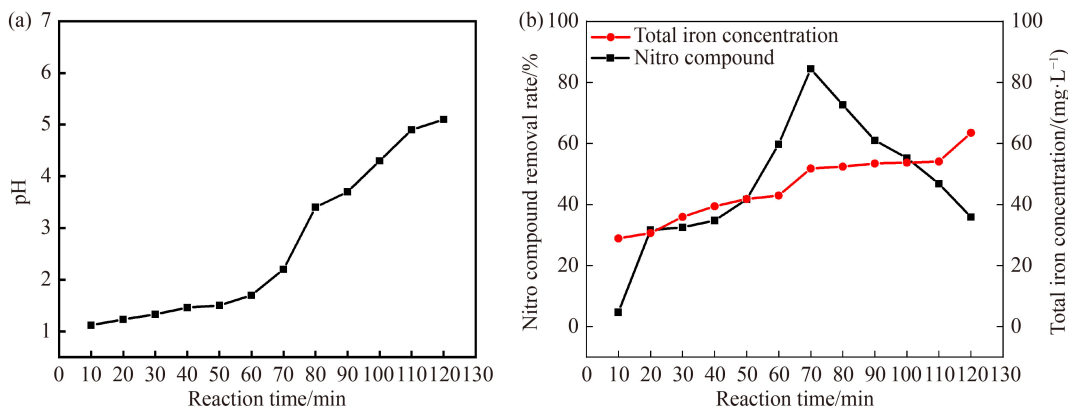


Fig. 2 Variations of (a) pH and (b) removal rate of nitro compounds and total iron concentration in the wastewater with reaction time (pH = 1.1, $Q = 80$ L·h⁻¹, $\beta = 104$).

react with OH^- in the solution to form $\text{Fe}(\text{OH})_3$, which can adsorb nitro compounds and then settle with iron sludge to form solid pollutants. After 80 min, the Fe concentration is low in the wastewater and the removal rate of nitro compounds fluctuates slightly, which is attributed to the low efficiency of Fe–C micro-electrolysis because of the formation of metal oxides on the surface of Fe–C packing. After 110 min, the pH is higher than 5 and a large amount of $\text{Fe}(\text{OH})_2$ and $\text{Fe}(\text{OH})_3$ are formed. In this case, the removal rate of nitro compounds is increased again as a result of Fe–C micro-electrolysis and the physical adsorption of $\text{Fe}(\text{OH})_2$ and $\text{Fe}(\text{OH})_3$.

In the following experiments, the reaction time is set to 100 min in order to avoid the adsorption and coagulation of $\text{Fe}(\text{OH})_2$ and $\text{Fe}(\text{OH})_3$ at high pH and the transfer of nitro compounds from the liquid phase to the solid phase. The high concentrations of Fe in the wastewater within 100 min provide sufficient Fe for subsequent Fenton oxidation. Thus, the waste can be utilized for wastewater treatment.

3.1.2 Effects of high-gravity factor

The high-gravity factor (β) is defined as the ratio of centrifugal acceleration to gravity acceleration, and it is used to describe the intensity of the high gravity field in RPB [34]:

$$\beta = \frac{2\pi^2 N^2 (r_1^2 + r_1 r_2 + r_2^2)}{3 \times 900 (r_1 + r_2) g}, \quad (2)$$

where r_1 (m) and r_2 (m) are the inner and outer radius of the packing, respectively, and N ($\text{r}\cdot\text{min}^{-1}$) is the rotor speed. Given that the inner and outer radius of the packing bed are constant, the high-gravity factor is proportional to the square of the rotor speed, and thus it can be adjusted by adjusting the rotation speed of the RPB.

Figure 3 shows the effects of high-gravity factor, liquid flow rate and initial pH of solution on the removal rate of nitro compounds and the total iron concentration in the solution. Figures 3(a) and 3(b) show the effect of high-gravity factor on the removal rate of nitro compounds and the total iron concentration under the conditions of $Q = 80 \text{ L}\cdot\text{h}^{-1}$ and $\text{pH} = 1.1$. Figure 3(a) shows that at a reaction time of 100 min, the removal rate of nitro compounds is increased from 46.6% to 63.1% as the high-gravity factor is increased from 11.56 to 46.22, after which it is decreased to 49.3% as the high-gravity factor is further increased to 104. The liquid can be sheared into smaller droplets and thinner films at larger high-gravity factors [35], which can reduce the diffusion resistance of the liquid and increase the liquid–solid mass transfer rate. As a result, more organic pollutants are adsorbed on the packing surface, which can increase the electron transfer between nascent $[\text{H}]$ and organic pollutants and the decomposition rate of organic pollutants by Fe–C

micro-electrolysis. Increasing the high-gravity factor can also accelerate the renewal of the interface, which can prevent the formation of metal oxides on the surface of Fe–C particles and thus extend their service life.

The liquid–solid mass transfer can be described as follows [36]:

$$k_s = 2.8 \left(\frac{Q_w}{\Delta x} \right) S_c^{-2/3} Re^{-8/9} Gr_{\text{avg}}^{2/9}. \quad (3)$$

The Grashof number (Gr) and Reynolds number (Re) are proportional to the rotation speed and the liquid flow rate, respectively. At $\beta < 46.22$, the liquid–solid mass transfer coefficient increases with increasing high-gravity factor, potentially resulting in an increase in the removal rate of nitro compounds; while at $\beta > 46.22$, the residence time of the liquid is too short to permit sufficient liquid–solid contact, potentially resulting in a decrease in the removal rate of nitro compounds. In this study, the optimal high-gravity factor is determined to be $\beta = 46.22$, at which the removal rate of nitro compounds reaches a maximum of 68.4%.

Similarly, the total Fe concentration also increases at first and then decreases with increasing high-gravity factor, as shown in Fig. 3(b). At low high-gravity factors, more metal oxides are deposited on the packing surface due to the low renewal rate, and consequently the efficiency of Fe–C micro-electrolysis is reduced. The total iron concentration reaches a maximum at $\beta = 46.22$, at which the removal rate of nitro compounds is still high due to physical adsorption of $\text{Fe}(\text{OH})_3$. At $\beta > 46.22$, the interface is renewed more quickly but the liquid–solid contact time is reduced with increasing high-gravity factor. In this case, the total iron concentration is low in the wastewater. Thus, the optimal high-gravity factor is determined to be 46.22.

3.1.3 Effects of liquid flow rate

Figures 3(c) and 3(d) show that under the conditions of $\text{pH} = 1.1$ and $\beta = 46.22$, the removal rate of nitro compounds and the total iron concentration increase with the increase of the liquid flow rate from 40 to 80 $\text{L}\cdot\text{h}^{-1}$, but decrease slightly with further increase of the liquid flow rate to 160 $\text{L}\cdot\text{h}^{-1}$. Increasing the liquid flow rate from 40 to 80 $\text{L}\cdot\text{h}^{-1}$ can increase the spraying density and the mixing efficiency of the solution, and the packing is thoroughly wet and the liquid holdup and the effective liquid–solid contact area are increased [37]. The liquid flow rate changes the spray density of the liquid, which is defined as the liquid volume sprayed per unit time on the unit cross-sectional area of the packed bed:

$$L = \frac{Q}{2\pi r h}, \quad (4)$$

$$L_{\text{min}} = L_w \cdot a, \quad (5)$$

where L is the average liquid spray density ($\text{m}^3\cdot\text{m}^{-2}\cdot\text{h}^{-1}$),

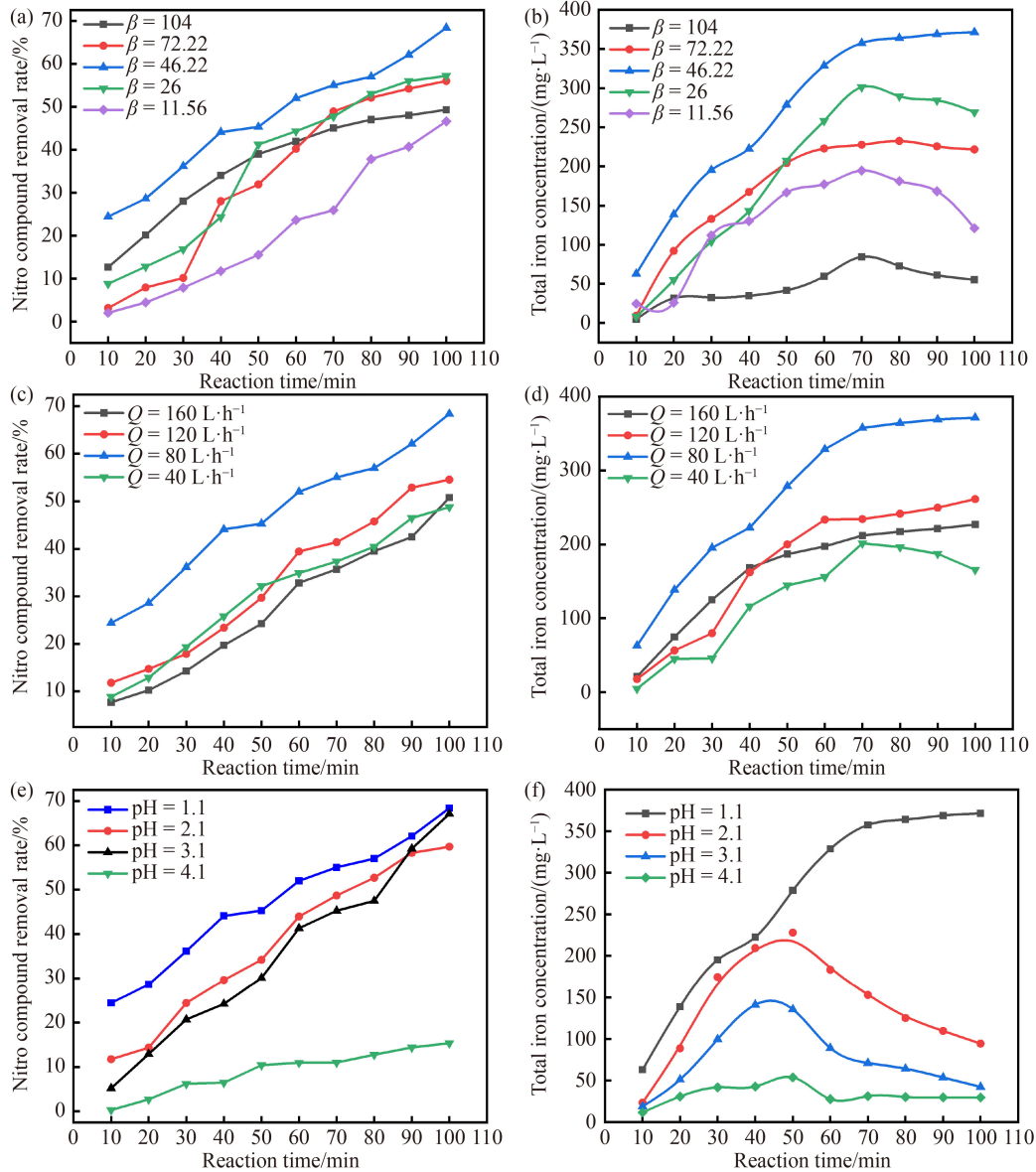


Fig. 3 Effects of operating parameters on the removal rate of nitro compounds and the total iron concentration in the solution: (a, b) high-gravity factor ($Q = 80 \text{ L}\cdot\text{h}^{-1}$, $\text{pH} = 1.1$), (c, d) liquid flow rate ($\beta = 46.22$, $\text{pH} = 1.1$), and (e, f) initial solution pH ($\beta = 46.22$, $Q = 80 \text{ L}\cdot\text{h}^{-1}$).

Q is the liquid flow rate ($\text{m}^3\cdot\text{h}^{-1}$), r is the rotor diameter (m), h is the rotor height, L_w is the minimum wetting rate ($0.08 \text{ m}^3\cdot\text{m}^{-1}$ for bulk packing), and a is the specific surface area of the packing layer. The minimum spray density is calculated to be $12.48 \text{ m}^3\cdot\text{m}^{-2}\cdot\text{h}^{-1}$. The packing is not completely wet at a liquid flow rate of $40 \text{ L}\cdot\text{h}^{-1}$ because the liquid spray density ($7.07 \text{ m}^3\cdot\text{m}^{-2}\cdot\text{h}^{-1}$) is lower than the minimum spray density. The packing is sufficiently wet as the liquid flow rate increases to $80 \text{ L}\cdot\text{h}^{-1}$ because the spray density ($14.15 \text{ m}^3\cdot\text{m}^{-2}\cdot\text{h}^{-1}$) is greater than the minimum spray density, and in this case the effective liquid–solid contact area is increased. Thus, the maximum removal rate of nitro compounds (68.4%) and total iron concentration ($371.5 \text{ mg}\cdot\text{L}^{-1}$) are obtained at $Q = 80 \text{ L}\cdot\text{h}^{-1}$. At liquid flow rates higher than $80 \text{ L}\cdot\text{h}^{-1}$,

the liquid droplets become larger and the films become thicker, which can inhibit the mass transfer of organic pollutants to the surface of Fe–C packing. These results indicate that the optimal liquid flow rate is $80 \text{ L}\cdot\text{h}^{-1}$.

3.1.4 Effects of initial solution pH

Figures 3(e) and 3(f) show that the effects of initial solution pH on the removal rate of nitro compounds and the total iron concentration under the conditions of $\beta = 46.22$ and $Q = 80 \text{ L}\cdot\text{h}^{-1}$. Figure 3(f) shows that the total iron concentration is lower at higher pH, and it shows a decreasing trend after 50 min at $\text{pH} = 2.1$ and 3.1 . Figure 3(e) shows that the removal rate of nitro compounds increases rapidly at $\text{pH} = 2.1$ and 3.1 , and the

final removal rate is approximately the same as that at pH = 1.1. However, the removal rate of nitro compounds at pH = 4.1 is lower than 20%, and the total iron concentration is lower than 50 mg·L⁻¹. The reduction reaction of nitro compounds by Fe–C micro-electrolysis is described as follows [38]:



As H⁺ participates in the reduction reaction of nitro compounds, an acidic environment where there is a high H⁺ concentration may favor Fe–C micro-electrolysis. The high H⁺ concentration at low pH contributes greatly to the electrochemical corrosion of Fe and makes it impossible to form Fe(OH)₂ and Fe(OH)₃ from Fe²⁺ and Fe³⁺. Thus, no iron sludge would be formed. At pH = 2.1 and 3.1, the pH of the Fe–C micro-electrolysis system increases as the reaction proceeds, and the total iron concentration is reduced after 50 min. A large amount of nitro compounds can be adsorbed by Fe(OH)₂ and Fe(OH)₃, which form floccules and then precipitate as iron sludge. Therefore, the nitro compounds can undergo reduction reaction by Fe–C micro-electrolysis and physical adsorption by Fe(OH)₂ and Fe(OH)₃. For this reason, no substantial difference is observed in the removal rate of nitro compounds between pH = 2.1 or 3.1 and pH = 1.1. At pH = 4.1, the H⁺ concentration is low and less [H] is generated in unit time, which can reduce the reduction reaction and consequently the removal rate of nitro compounds. Considering the cost involved in pH adjustment and treatment of iron sludge, the optimal initial solution pH is set to 1.1.

3.2 Comparison between RPB and STR

The Fe–C materials prepared in the same batch are continuously used for the treatment of 2 L of dinitrotoluene wastewater in RPB (pH = 1.1, *t* = 100 min, β = 46.22, and *Q* = 80 L·h⁻¹) and STR (pH = 1.1, *t* = 100 min, and stirring rate = 200 r·min⁻¹) for 4 cycles. Note that no treatment is given to the Fe–C packing in the replacement of wastewater.

Figure 4 shows that in the single-cycle experiment, the removal rate of nitro compounds in RPB is always higher than that in STR. However, it is noted that the difference is negligible before 50 min, after which the difference becomes more apparent with increasing reaction time. This is because the removal rate of nitro compounds increases continuously at approximately the same rate in RPB but at a much slower rate in STR. In RPB where there is a large liquid–solid contact area, the diffusion rate of nitro compounds to the surface of Fe–C packing and the electron transfer rate of Fe are higher compared with that in STR. However, the pH of the Fe–C micro-electrolysis system is increased after 60 min, and thus Fe(OH)₂, Fe(OH)₃ and other iron oxides are formed from Fe²⁺ and Fe³⁺ and then adsorbed on the packing surface,

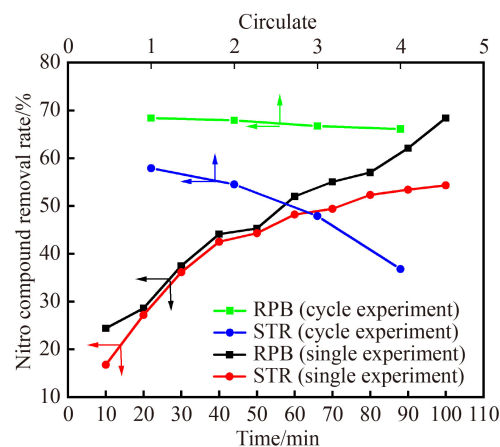


Fig. 4 Comparison between RPB and STR in single and cycling experiments (pH = 1.1, *t* = 100 min; for RPB: β = 46.22, *Q* = 80 L·h⁻¹; for STR: *r* = 200 r·min⁻¹).

which can reduce the liquid–solid contact area. In STR, the impurities on the packing surface could not be sufficiently removed and thus less active sites are available for degradation of dinitrotoluene. As a result, the removal rate of nitro compounds is lower in STR. In RPB, the high-speed rotating packing causes liquid disturbance and increases surface renewal and liquid–solid contact, and thus the metal oxides can be easily detached from the packing surface. As a result, more active sites are available to maintain the high electrolytic efficiency in RPB.

In the four-cycle experiment, the removal rate of nitro compounds is maintained at about 68% after four cycles in RPB, but it is decreased from 57% to 38% in STR. This is because the reduction reaction of nitro compounds occurs on the packing surface, and the presence of impurities on the packing surface can reduce the effective liquid–solid contact area. Thus, the efficiency of Fe–C micro-electrolysis in STR is reduced rapidly with the increase of cycle, while the efficiency is improved and the service time of Fe–C particles is extended in RPB due to its potential to remove the impurities on the packing surface and increase the liquid–solid contact area.

3.3 Analysis of Fe–C packing by scanning electron microscopy (SEM) and energy dispersive X-ray spectroscopy (EDX)

The same volumes of Fe–C packing are used for treatment of dinitrotoluene wastewater for 4 cycles in RPB and STR and then characterized by SEM and EDX. Figure 5 shows the SEM images and EDX spectra of the Fe–C packing before and after use. Figure 5(a) shows that the fresh Fe–C packing has a clean and smooth surface without any impurities, and it is mainly composed of C (4.04%) and Fe (75.49%). Figure 5(b) shows that the Fe–C packing used for four cycles in STR has a block-like and rather coarse surface with obvious gaps between

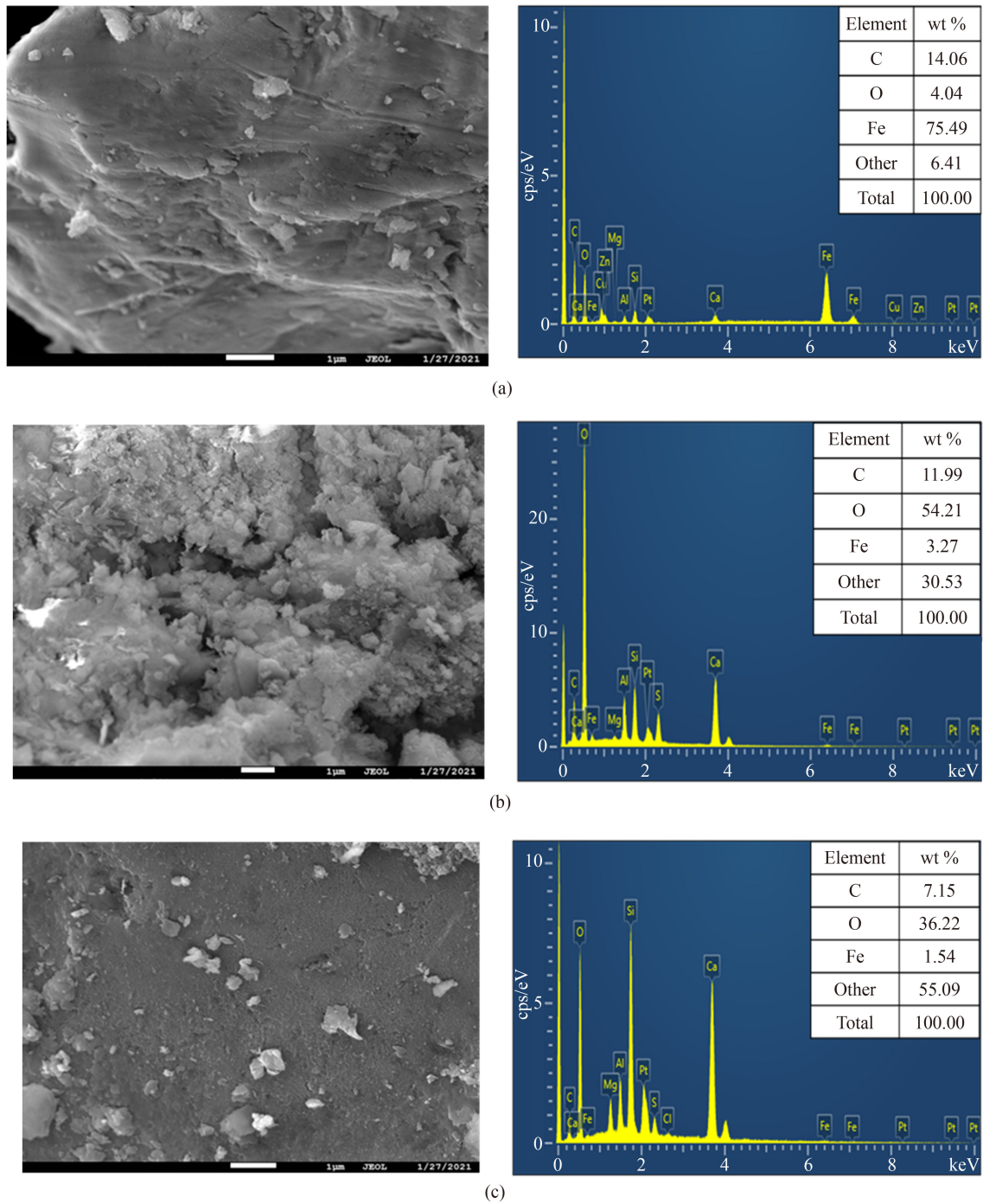


Fig. 5 SEM images and EDX spectra of Fe-C packing: (a) fresh Fe-C packing; Fe-C packing used for four cycles in (b) STR and (c) RPB.

blocks. The O content is increased to 54.21%, indicating that the blocks on the surface are metal oxides. Figure 5(c) shows that the Fe-C packing used for four cycles in RPB has a rough but clean surface with few iron oxides and densely distributed holes resulting from the detachment of Fe-C packing after acid corrosion. Overall, no substantial difference is observed in the surface morphology between fresh and used Fe-C packing in RPB, and the active sites on the packing surface can be adequately exposed. It is also noted that the O element (36.22%) is lower than that

in STR, which indicates that there are fewer metal oxides on the surface. Thus, it can be concluded that RPB can keep the surface of Fe-C packing clean throughout the reaction with a low amount of O-containing impurities.

3.4 Degradation mechanism of dinitrotoluene wastewater by Fe-C micro-electrolysis

Gas chromatography-mass spectrography (GC-MS) was performed to determine the compositions of

dinitrotoluene wastewater, and the results are shown in Fig. 6 and Table 2.

The GC-MS results reveal that there exist many nitro compounds in addition to dinitrotoluene (Table 2), which are mainly nitroaromatic compounds. Here, the removal rate of nitro compounds is used to indicate the effect of Fe–C micro-electrolysis, and the degradation mechanism of dinitrotoluene wastewater by Fe–C micro-electrolysis is investigated using nitrobenzene as the model pollutant. To this purpose, 200 mg·L⁻¹ nitrobenzene solution was prepared and the pH was adjusted to that of dinitrotoluene wastewater, and then the high-gravity intensified Fe–C micro-electrolysis was carried out under optimal operating conditions. As seen from Fig. 7, the characteristic peak of nitrobenzene is observed at 267 nm. However, the absorbance is gradually decreased over

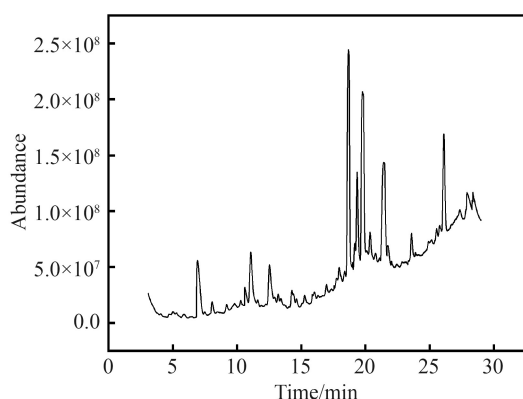


Fig. 6 Gas chromatogram of dinitrotoluene wastewater.

Table 2 Compositions of dinitrotoluene wastewater

No.	Retention time/min	Compound	Mass spectrometry (<i>m/z</i>)
1	6.71–6.92	Nitrobenzene	123.1
2	10.94–11.07	3-Nitrotoluene	137.14
3	18.59–18.68	Dinitrotoluene	182.13
4	19.24–19.35	2,4-Dinitrobenzene	168.11
5	19.68–19.76	2,6-Dinitrotoluene	182.13

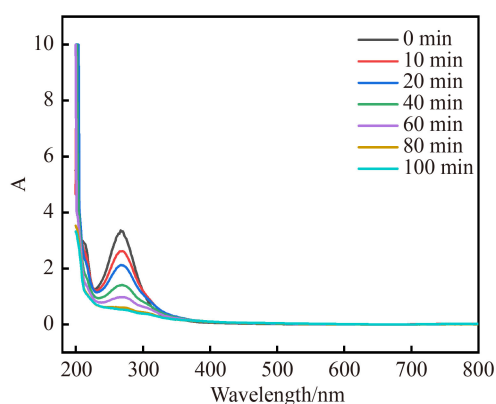


Fig. 7 High-gravity intensified Fe–C micro-electrolysis for degradation of nitrobenzene by ultraviolet–visible spectroscopy (pH = 1.1, $t = 100$ min, $\beta = 46.22$, $Q = 80$ L·h⁻¹).

time, and no other peaks are observed at 100 min.

To further elucidate the degradation mechanism, the intermediates were detected using GC–MS at different times. As shown in Fig. 8 and Table 3, aniline, nitrosobenzene and azobenzene are detected. The possible mechanism is deduced from the GC–MS results (Fig. 8), and the possible intermediates are shown in Table 3.

Figure 9 shows the complete degradation pathway of nitrobenzene reduction by Fe–C micro-electrolysis. The reactions I–III are the main reactions. The nitro group is converted into the nitroso group with the addition of two electrons and the loss of one water molecule, which in turn is reduced into hydroxyl aniline with the addition of another two electrons. Finally, aniline is obtained with the addition of two electrons. Thus, a total of six electrons are transferred in reactions I–III [18]. Azobenzene is also detected by GC–MS. Thus, condensation reaction (reactions III–IV) may also occur [39], corresponding to the one-step conversion of aniline (reactions IV–VI).

It is worth noting that there is abundant nitrosobenzene when the reaction time is 10 min (Fig. 8). According to Fig. 7, the nitrobenzene concentration is significantly decreased at 10 min, indicating that a large amount of nitrosobenzene is reduced to nitrobenzene by Fe–C packing at the beginning of the reaction. Hydroxylaniline is an intermediate product formed in the reduction of nitrobenzene. Almost no hydroxylaniline is detected in the reduction of nitrobenzene using Fe–C micro-electrolysis [40]. As shown in Fig. 10, the nitrobenzene concentration is decreased from the initial 200 to 40 mg·L⁻¹ at 10 min of the reaction, but aniline is not detected until 20 min of the reaction.

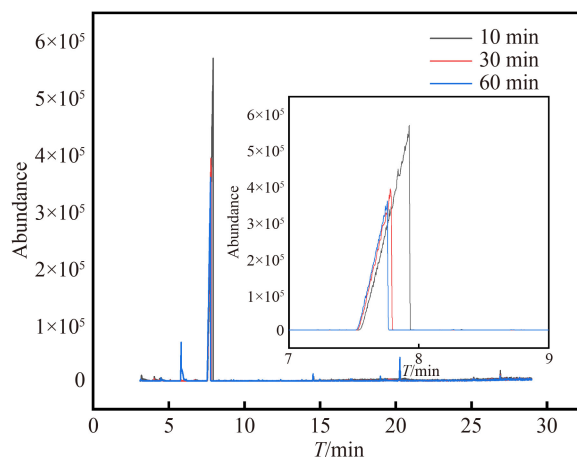


Fig. 8 GC–MS analysis of high-gravity intensified Fe–C micro-electrolysis for degradation of nitrobenzene.

Table 3 Intermediates by GC–MS

No.	Retention time/min	Compound	Mass spectrometry (<i>m/z</i>)
1	5.76–6.05	Aniline	93.13
2	7.56–7.94	Nitrosobenzene	107.11
3	20.14–20.31	Azobenzene	182.22

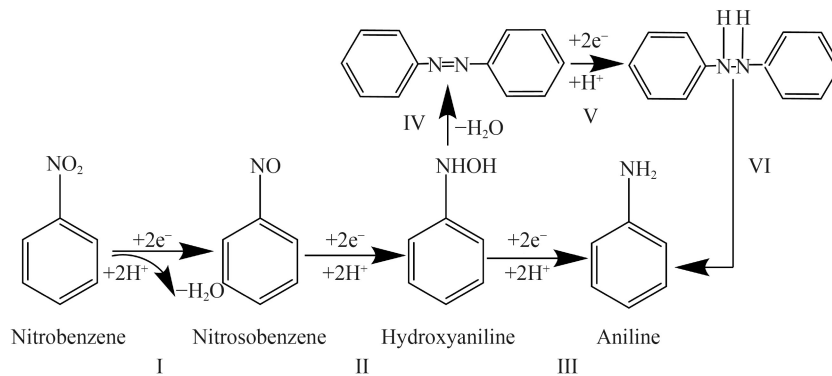


Fig. 9 Degradation mechanism of nitrobenzene by Fe-C micro-electrolysis.

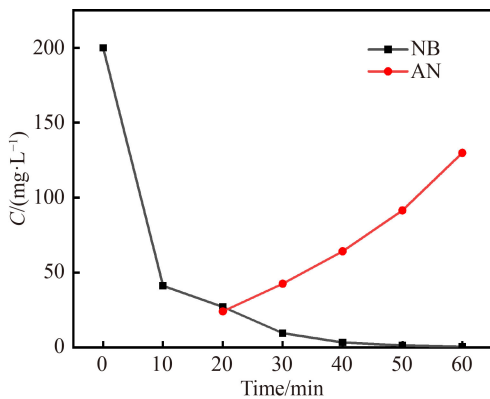
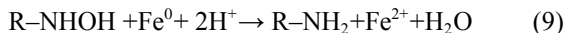
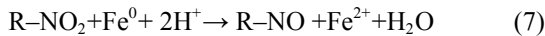


Fig. 10 Changes in the concentration of nitrobenzene and aniline (pH = 1.1, t = 60 min, β = 46.22, Q = 80 L·h⁻¹).

The standard redox potentials (E^0) of nitrobenzene and aniline are -0.485 and 1.030 V; and the standard molar Gibbs energies of nitrobenzene, nitrosobenzene, phenylhydrazine, aniline and water ($\Delta_r G^0$) are 146.2, 201.3, 303.33, 149.1 and -237.1 kJ·mol⁻¹, respectively. The reduction of nitrobenzene by Fe-C micro-electrolysis can be described by Eqs. (7)–(9) according to the intermediate products [18]:



The standard molar reaction Gibbs energies ($\Delta_r G^0$) in Eqs. (7)–(9) can be calculated from $\Delta_r G^0$, and then the standard oxidation–reduction potential (E^0) of each substance is obtained using Eq. (10):

$$\Delta_r G^0 = zFE^0, \quad (10)$$

where z is the number of electrons transferred in the reaction, and F is the Faraday constant (96485 C·mol⁻¹). Finally, the oxidation–reduction potential (E) under the reaction conditions is calculated according to Nernst Eq. (11):

$$E = E^0 - \frac{RT}{zF} \ln \Pi_B a_B^{v_B}, \quad (11)$$

where R is the gas constant (8.314 J·mol⁻¹·K⁻¹), and T is the reaction temperature (K). Then the oxidation–reduction potential difference (ΔE) of Eqs. (7)–(9) is calculated [41].

The ΔE from nitrobenzene to nitrosobenzene (Fig. 9, reaction I), from nitrosobenzene to hydroxyaniline (Fig. 9, reaction II), and from hydroxyaniline to aniline (Fig. 9, reaction III) is calculated to be 1.42, -1.46 , and 1.55 V, respectively. Thus, the reduction of nitrosobenzene to hydroxyaniline is the most unfavorable, whereas the ΔE of reaction I and reaction III are beneficial to the reaction. Thus, nitrobenzene is quickly converted to nitrosobenzene at the beginning of the reaction, which is unlikely to be converted to hydroxyaniline and thus leads to the accumulation of nitrosobenzene. It is easy for the reduction of hydroxyaniline to aniline, and thus the concentration of hydroxyaniline is relatively low.

4 Conclusions

- (1) The removal rate of nitro compounds is maintained at approximately 68% after 4 cycles in RPB, but it is decreased substantially from 57.9% to 36.8% in STR. The efficiency of Fe-C micro-electrolysis is improved and the service time of Fe-C particles is extended in RPB due to its potential to remove the impurities on the packing surface and increase the liquid–solid contact area.
- (2) The Fe-C packing in RPB has a cleaner surface and lower contents of Fe and O elements compared with that in STR. As the impurities on the packing surface can be sufficiently removed in RPB, more reactive sites are regenerated for subsequent degradation of dinitrotoluene.
- (3) The optimal conditions for treatment of 200 mg·L⁻¹ dinitrotoluene wastewater by high-gravity intensified Fe-C micro-electrolysis are as follows: high-gravity factor $\beta = 46.22$, liquid flow $Q = 80$ L·h⁻¹, initial pH = 1.1, and reaction time = 100 min, under which the removal rate of nitro compounds reaches 68.4%.
- (4) Fe-C micro-electrolysis can be used as a low-cost and effective method for treatment of dinitrotoluene wastewater, and it can convert nitro compounds that are difficult to degrade

into easily biodegradable amino compounds. (5) The nitro compounds can be degraded by high-gravity intensified Fe–C micro-electrolysis, and the intermediate products include nitrosobenzene, benzene hydroxylamine and azobenzene.

Acknowledgements This work was supported by the Fund for Shanxi “1331 Project” (Grant No. nuc2021-006), Scientific Activities of Selected Returned Overseas Professionals in Shanxi Province (Grant No. 20200004) and Shanxi Scholarship Council of China (Grant No. 2019032).

References

- Guo N, Li Y P. Reaction mechanism and influence factors of treating dinitrotoluene wastewater by wet air oxidation. *Chinese Journal of Explosives and Propellants*, 2010, 33(3): 25–29 (In Chinese)
- Fierke M A, Olson E J, Buhlmann P, Stein A. Receptor-based detection of 2,4-dinitrotoluene using modified three-dimensionally ordered macroporous carbon electrodes. *ACS Applied Materials & Interfaces*, 2012, 4(9): 4731–4739
- Rodgers J D, Bunce N J. Treatment methods for the remediation of nitroaromatic explosives. *Water Research*, 2001, 35(9): 2101–2111
- Chen W S, Chiang W C, Wei K M. Recovery of nitrotoluenes from wastewater by solvent extraction enhanced with salting-out effect. *Journal of Hazardous Materials*, 2007, 147(1–2): 197–204
- Rajagopal C, Kapoor J C. Development of adsorptive removal process for treatment of explosives contaminated wastewater using activated carbon. *Journal of Hazardous Materials*, 2001, 87(1–3): 73–98
- Li F L, Chen C, Wang Y D, Li W P, Zhou G L, Zhang H Q, Zhang J, Wang J T. Activated carbon-hybridized and amine-modified polyacrylonitrile nanofibers toward ultrahigh and recyclable metal ion and dye adsorption from wastewater. *Frontiers of Chemical Science and Engineering*, 2021, 15(4): 984–997
- Abramov V O, Abramov O V, Gekhman A E, Kuznetsov V M, Price G J. Ultrasonic intensification of ozone and electrochemical destruction of 1,3-dinitrobenzene and 2,4-dinitrotoluene. *Ultrasonics Sonochemistry*, 2006, 13(4): 303–307
- Chen W S, Lin S Z. Destruction of nitrotoluenes in wastewater by electro-Fenton oxidation. *Journal of Hazardous Materials*, 2009, 168(2–3): 1562–1568
- Jiao W Z, Shao S J, Yang P Z, Gao K C, Liu Y Z. Kinetics and mechanism of nitrobenzene degradation by hydroxyl radicals-based ozonation process enhanced by high gravity technology. *Frontiers of Chemical Science and Engineering*, 2021, 15(5): 1197–1205
- Song Y J, Zhong S Q, Li Y J, Dong K, Luo Y, Chu G W, Zou H K, Sun B C. Study on the catalytic degradation of sodium lignosulfonate to aromatic aldehydes over nano-CuO: process optimization and reaction kinetics. *Chinese Journal of Chemical Engineering*, 2022, in press
- Paca J, Halecky M, Barta J, Bajpai R. Aerobic biodegradation of 2,4-dinitrotoluene and 2,6-dinitrotoluene: performance characteristics and biofilm composition changes in continuous packed-bed bioreactors. *Journal of Hazardous Materials*, 2009, 163(2–3): 848–854
- Christopher H J, Boardman G D, Freedman D L. Aerobic biological treatment of 2,4-dinitrotoluene in munitions plant wastewater. *Water Research*, 2000, 34(5): 1595–1603
- Parham H S, Saeed S. Simultaneous removal of nitrobenzene, 1,3-dinitrobenzene and 2,4-dichloronitrobenzene from water samples using anthracite as a potential adsorbent. *Journal of Environmental Chemical Engineering*, 2013, 1(4): 1117–1123
- Arowo M, Zhao Z M, Li G J, Chu G W, Sun B C, Shao L. Ozonation of *o*-phenylenediamine in the presence of hydrogen peroxide by high-gravity technology. *Chinese Journal of Chemical Engineering*, 2018, 26(3): 601–607
- Chamarro E, Marco A, Esplugas S. Use of Fenton reagent to improve organic chemical biodegradability. *Water Research*, 2001, 35(4): 1047–1051
- El Shafei G M S, Yehia F Z, Dimitry O I H, Badawi A M, Eshaq G. Ultrasonic assisted-Fenton-like degradation of nitrobenzene at neutral pH using nanosized oxides of Fe and Cu. *Ultrasonics Sonochemistry*, 2014, 21(4): 1358–1365
- Bagal M V, Gogate P R. Wastewater treatment using hybrid treatment schemes based on cavitation and Fenton chemistry: a review. *Ultrasonics Sonochemistry*, 2014, 21(1): 1–14
- Agrawal A, Tratnyek P. Reduction of nitro aromatic compounds by zero-valent iron metal. *Environmental Science & Technology*, 1995, 30(1): 153–160
- Yang S, Liang Z, Yu H, Wang Y, Chen Y. Chemical oxygen demand removal efficiency and limited factors study of aminosilicone polymers in a water emulsion by iron-carbon micro-electrolysis. *Water Environment Research*, 2014, 86(2): 156–162
- Lai B, Zhou Y X, Yang P, Yang J H, Wang J L. Degradation of 3,3'-iminobis-propanenitrile in aqueous solution by Fe⁰/GAC micro-electrolysis system. *Chemosphere*, 2013, 90(4): 1470–1477
- Zhao H D, Nie T N, Zhao H X, Liu Y, Zhang J, Ye Q, Xu H, Shu S H. Enhancement of Fe–C micro-electrolysis in water by magnetic field: mechanism, influential factors and application effectiveness. *Journal of Hazardous Materials*, 2020, 410: 124643
- Liu H N, Li G T, Qu J H, Liu H J. Degradation of azo dye acid orange 7 in water by Fe⁰/granular activated carbon system in the presence of ultrasound. *Journal of Hazardous Materials*, 2007, 144(1–2): 180–186
- Zhou H, Lv P, Shen Y, Wang J, Fan J. Identification of degradation products of ionic liquids in an ultrasound assisted zero-valent iron activated carbon micro-electrolysis system and their degradation mechanism. *Water Research*, 2013, 47(10): 3514–3522
- Hung H M, Hoffmann M R. Kinetics and mechanism of the enhanced reductive degradation of CCl₄ by elemental iron in the presence of ultrasound. *Environmental Science & Technology*, 1998, 32(19): 3011–3016
- Zhang W H, Wang D, Wang J X, Pu Y, Chen J F. High-gravity-assisted emulsification for continuous preparation of waterborne polyurethane nanodispersion with high solids content. *Frontiers*

- of Chemical Science and Engineering, 2020, 14(6): 1087–1099
26. Jiao W Z, Luo S, He Z, Liu Y Z. Applications of high gravity technologies for wastewater treatment: a review. *Chemical Engineering Journal*, 2017, 313: 912–927
 27. Fang L, Sun Q, Duan Y H, Zhai J, Wang D, Wang J X. Preparation of transparent BaSO₄ nanodispersions by high-gravity reactive precipitation combined with surface modification for transparent X-ray shielding nanocomposite films. *Frontiers of Chemical Science and Engineering*, 2021, 15(4): 902–912
 28. Lin C C, Liu W T. Ozone oxidation in a rotating packed bed. *Journal of Chemical Technology and Biotechnology (Oxford, Oxfordshire)*, 2003, 78(2–3): 138–141
 29. Cheng H H, Tan C S. Removal of CO₂ from indoor air by alkanolamine in a rotating packed bed. *Separation and Purification Technology*, 2011, 82: 156–166
 30. Wei X Y, Shao S J, Ding X, Jiao W Z, Liu Y Z. Degradation of phenol with heterogeneous catalytic ozonation enhanced by high gravity technology. *Journal of Cleaner Production*, 2020, 248: 119179
 31. Liu W L, Jiao W Z, Liu Y Z, Gao J, Su Q, Li J, Guo L, Xu C C. Treatment of dinitrotoluene production wastewater by iron-carbon micro-electrolysis method. *Chinese Journal of Explosives and Propellants*, 2014, 37(3): 33–38 (In Chinese)
 32. Meyer D, Prien R D, Dellwig O, Connelly D P, Schulz-Bull D E. *In situ* determination of iron (II) in the anoxic zone of the central Baltic Sea using ferene as spectrophotometric reagent. *Marine Chemistry*, 2012, 130: 21–27
 33. Hung H M, Hoffmann M R. Kinetics and mechanism of the enhanced reductive degradation of nitrobenzene by elemental iron in the presence of ultrasound. *Environmental Science & Technology*, 2000, 32(19): 3011–3016
 34. Li P Y, Wei X Y, Shao S J, Gao W Q, Jing J X, Jiao W Z, Liu Y Z. Degradation of nitrobenzene in wastewater by O₃/FeOOH in a rotating packed bed. *Chemical Engineering and Processing*, 2020, 153: 107981
 35. Shao S, Lei D, Song Y, Liang L, Liu Y, Jiao W. Cu–MnO_x/γ-Al₂O₃ catalyzed ozonation of nitrobenzene in a high-gravity rotating packed bed. *Industrial & Engineering Chemistry Research*, 2012, 60(5): 2123–2135
 36. Panda M, Bhowal A, Datta S. Removal of hexavalent chromium by biosorption process in rotating packed bed. *Environmental Science & Technology*, 2011, 45(19): 8460–8466
 37. Chen G, Zhu X, Chen R, Liao Q, Ye D D, Feng H, Liu J, Liu M. Gas–liquid–solid monolithic microreactor with Pd nanocatalyst coated on polydopamine modified nickel foam for nitrobenzene hydrogenation. *Chemical Engineering Journal*, 2018, 334: 1897–1904
 38. Jiao W Z, Feng Z R, Liu Y Z. Treatment of nitrobenzene-containing wastewater by iron–carbon micro-electrolysis. *Journal of Nanoparticle Research*, 2016, 66: 1150–1155
 39. Mu Y, Yu H Q, Zheng J C, Zhang S J, Sheng G P. Reductive degradation of nitrobenzene in aqueous solution by zero-valent iron. *Chemosphere*, 2004, 54(7): 789–794
 40. Lee H, Kim B H, Park Y K, Kim S J, Jung S C. Application of recycled zero-valent iron nanoparticle to the treatment of wastewater containing nitrobenzene. *Journal of Nanomaterials*, 2015, 16: 363–341
 41. Cai Z Q, Fu J, Du P H, Zhao X, Hao X D, Liu W, Zhao D Y. Reduction of nitrobenzene in aqueous and soil phases using carboxymethyl cellulose stabilized zero-valent iron nanoparticles. *Chemical Engineering Journal*, 2018, 332: 227–236